Weld Heat-Affected-Zone Response to Elevated-Temperature Deformation

Constant-displacement-rate testing yields service-performance estimates for HAZ microstructures in 2.25Cr-1Mo steel

BY R. J. BOWERS AND E. F. NIPPES

ABSTRACT. The mechanical response to elevated-temperature deformation was assessed for weld heat-affected-zone (HAZ) and base-metal microstructures in 2.25Cr-1Mo steel. A constant-displacement-rate (CDR) test, capable of determining long-time, notch-sensitivity tendencies, was implemented on a Gleeble 1500 thermal/mechanical simulator and an Instron. Microstructures representative of the coarse-grained, grain-refined, and intercritical regions of the HAZ were simulated on a Gleeble. Microstructural reproduction reflected the preheat and postweld heat treatments in accordance with the required codes.

A K_I analysis of the data was conducted, which showed that small-scale yielding criteria were adhered to throughout the test. The highest K_I values were found for the base metal. Failure occurred at the peak load for the coarse-grained microstructural region; no K_I analysis was possible. An empirically derived relationship for CrMoV steels between the displacement-at-failure value in the CDR test and the estimated service life was employed. Both the Gleeble and Instron tests showed the coarse-grained region to have the shortest estimated service life.

The test results indicated that the high-temperature extensometer control of the Instron was better able to maintain stable crack growth after peak load than the crosshead control of the Gleeble. The CDR test was seen to be an effective, short-time procedure to delineate and compare the strength and relative service life of the structures present in the weld HAZ.

R. J. BOWERS, now with Edison Welding Institute, Columbus, Ohio, was an Instructor in the Materials Science and Engineering Department at Rensselaer Polytechnic Institute, Troy, N.Y., at the time of this research. E. F. NIPPES is Professor Emeritus in the Materials Science and Engineering Department at Rensselaer Polytechnic Institute.

This work was funded by a graduate research fellowship from the American Welding Society.

KEY WORDS

Heat-Affected Zone
Elevated-Temperature
Mechanical Testing
2.25Cr-1Mo Steel
Life Assessment
Gleeble
K_I

Introduction

The HAZ of a weld is defined as that portion of the base metal that has not been melted but whose microstructure and properties have been altered by the welding process. The effect of welding thermal cycles on the microstructure and mechanical properties of the HAZ has been studied for a variety of metals. Of particular interest have been impact properties of the HAZ. The traditional approach of such studies has been to correlate the room-temperature mechanical response with the microstructure and its corresponding thermal cycle.

For Cr-Mo steels, investigation has centered on creep-rupture properties. These materials have found common use in elevated-temperature piping and pressure-vessel components. The results of creep rupture testing are plotted as rupture stress vs. the Larson-Miller Parameter. Evaluation of test data is accomplished by a comparison to the established data, such as ASTM DS 6S2 for 2.25Cr-1Mo steel (Ref. 1).

Lundin, *et al.* (Refs. 2–4), have conducted extensive work in the elevated-temperature properties of Cr-Mo steels. This research has included repair and evaluation of service-exposed material, as well as an examination of carbide morphology and distribution in new and service-exposed material.

In light of past research, it is possible to make certain generalizations about the room-temperature properties of the three major regions of the HAZ in ferrous alloys: the coarse-grained, grain-refined, and intercritical regions. The coarse-grained region has the lowest strength and toughness, whereas the grain-refined region possesses the highest strength and the lowest ductile-to-brittle transition temperature. The properties of the intercritical region depend largely upon the amount of transformation and whether martensite was produced during cooling.

Although these room-temperature properties are well known, no systematic study has been undertaken to characterize the HAZ response to elevated-temperature deformation. Because creep rates generally decrease with increasing grain size at elevated temperature, the creep resistance of the coarse-grained region may show improvement compared to the other regions at higher temperatures.

It was the intent of this investigation to assess the mechanical response of the HAZ and base-metal microstructures to elevated-temperature deformation in 2.25Cr-1Mo steel, which is commonly used in pressure-vessel and piping applications at elevated temperatures. A constant-displacement-rate (CDR) test was employed to evaluate the tendencies of the various heat-affected-zone regions to embrittle in long-time, stress-rupture tests.

Material

The 2.25Cr-1Mo alloy steel, pressure-vessel plate, ASME specification SA-387Gr22-Class 2, was used in this investigation. The plate thickness was 19 mm (0.75 in.). The specification for this steel requires a minimum yield strength of 310 MPa (45 ksi), a tensile strength range of 515–690 MPa (75–100 ksi) and a minimum reduction in area of 40%. The vendor-supplied mechanical properties in the transverse direction were: 478 MPa (69 ksi) yield strength, 585 MPa (85 ksi) tensile strength and 41.2% reduction in area. The composition of the steel is given in Table 1.

Material was supplied in the normalized-and-tempered condition. The plate was austenitized at 920°C (1688°F) for 2.5 min per mm of thickness and air cooled. This was followed by a 730°C (1346°F) temper for 3 h in air. The as-received, tempered-bainite microstructure is shown in Fig. 1. The prior-austenitic-grain diameter in the transverse direction was 22 µm (ASTM grain size 8) as measured by the line-intercept method. A hardness value of HV 191 (500 g, 15 s) was obtained as the average of eight readings.

Thermal-Cycle Simulation

Experimental Procedure

Cylindrical bars were machined from the as-received plate for subsequent thermal-cycle simulation. The rolling direction was along the longitudinal axis of the bars. An oversized radius allowed for finish machining after thermal-cycle simulation.

The 0.25-mm (0.010-in.), two-wire, chromel-alumel thermocouples were percussion welded to the cylindrical test bars. The thermocouple-base metal joint was later removed during final machining of the notch in the specimen. The bars were thermally cycled in air in a Gleeble with a 20-mm (0.8-in.) jaw spacing. The water-cooled Gleeble jaws extract heat from the test bar. Jaw separations of 25–32 mm (1–1.25 in.) are common; a reduced spacing was used in this instance to obtain the severe cooling rates associated with welding.

HAZ thermal cycles were simulated using the results of the method of Nippes, Merrill and Savage (Ref. 5) to represent a weld with an energy input of 3.0 kJ/mm (76.2 kJ/in.). Exact thermal cycles were determined from data originally acquired for arc welds in 25-mm (1-in.), carbon-steel plate. The use of these data has been extended to ferrous materials with low alloy concentrations.

Welding codes (Ref. 6) specify preheat temperatures for the plate during welding to reduce subsequent cooling rates and thereby avoid the formation of hard, brittle martensite. A minimum preheat of 150°C (300°F) is prescribed, with higher temperatures recommended for plate thicknesses above 19 mm (0.75 in.). The simulated thermal cycles were representative of a weld in 25-mm plate and reflected the use of a 250°C (480°F) preheat.

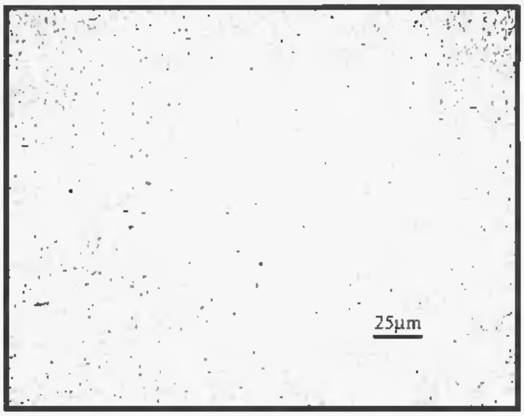

Fig. 1 — As received, tempered-bainitic microstructure, transverse direction. 4% Picral.

Postweld heat treatment (PWHT) acts to ameliorate the effects of residual stress or any martensite that may have formed. Codes require a 690°C–750°C (1275°–1375°F) PWHT for 2 min per mm of thickness, with a minimum of 15 min. Temperatures at the low end of this range are used by the power-generation industries to promote creep and rupture strength. Temperatures at the upper end of the PWHT range are used to promote resistance to corrosion and hydrogen embrittlement, which is necessary in the petrochemical industries.

The PWHT temperature used in this study was 690°C (1275°F), which is midway between the base-metal tempering temperature of 730°C (1346°F) and the CDR testing temperature of 650°C (1202°F). Subsequent to PWHT, the cylindrical bars were finish-machined into CDR test specimens — Fig. 2.

Material Response

During the welding process, the peak temperature experienced by the base plate decreases with distance from the weld centerline. The resulting range of peak temperatures gives rise to distinct microstructural regions within the HAZ. Two methods of quantifying thermal cycles in steels are to specify the time required to cool from 800° to 500°C (1472° to 932°F) and to reference the cooling rate at 480°C (900°F). The former relates to the time available for the nucleation and growth of pearlite to occur; the latter indicates the cooling rate near the knee of the continuous-cooling-transformation curve. In this investigation, three HAZ microstructural regions were simulated — Fig. 3.

During simulation of the coarse-grained region, the base metal was com-

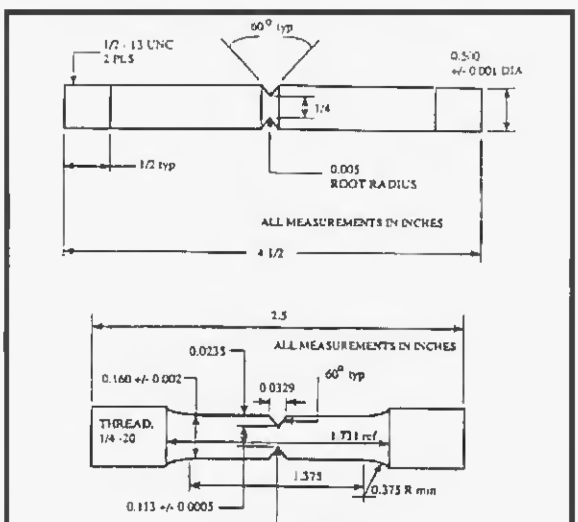

Fig. 2 — Gleeble (top) and Instron CDR test specimens.

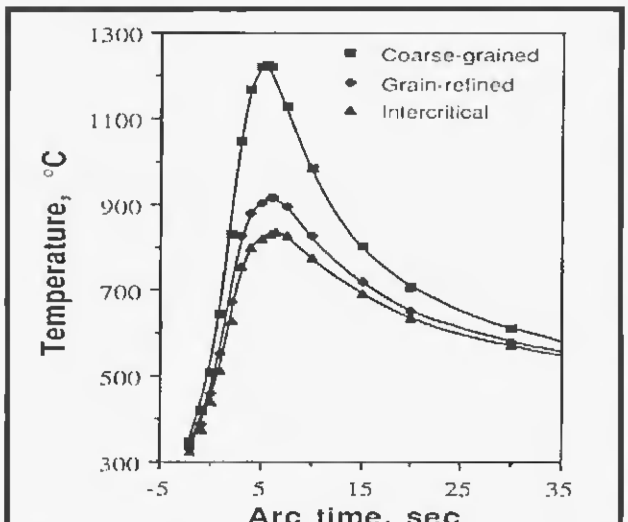

Fig. 3 — HAZ thermal cycles used in Gleeble microstructural simulation.

Table 1 — As-Received Composition of ASTM SA-387-GR22

Element	Weight-%
carbon	0.130
chromium	2.201
molybdenum	0.910
silicon	0.217
manganese	0.500
sulfur	0.013
phosphorus	0.013
copper	0.234
nickel	0.100
vanadium	0.002
niobium	0.001
iron	balance

pletely transformed to austenite during heating. The peak temperature of 1225°C (2237°F), which corresponds to a position high in the austenite phase field, allowed grain growth to occur. The 800° to 500°C cooling time was 42.5 s; the cooling rate at 480°C was 1.9°C/s (3.4°F/s). Upon cooling, these coarsened grains transformed to bainite — Fig. 4A. The prior austenitic grain size was 31 μm (ASTM 7). The hardness of the as-simulated microstructure was HV 351; after PWHT (Fig. 4B), the hardness of this structure had decreased to HV 247.

The peak temperature for the simulation of the grain-refined region, 915°C (1679°F), was located just above the A_3 transformation; this simulation limited the amount of time and temperature in the austenite phase field. Although the microstructure completely transformed to austenite, there was no substantial grain growth. The cooling time from 800°–500°C was 42.8 s; the cooling rate at 480°C was 1.9°C/s. Figure 5A shows the bainitic structure formed upon cooling. The prior-austenitic grain size in the transverse direction was 16 μm (ASTM 9). The as-simulated hardness was HV 350; after PWHT (Fig. 5B), the value was HV 210.

The peak temperature for the intercritical-region simulation, 835°C (1535°F), fell between the A_1 and A_3 temperatures. As such, the bainitic structure only partially transformed to austenite. The percentage of transformation was measured at 40% by the point-count method. The grain size of these transformed regions was 13 μm (ASTM 9.5). The 800° to 500°C cooling time was 43.4 s; the cooling rate at 480°C was 1.9°C/s. The significance of these values is diminished, however, because of the incomplete transformation. The structures upon cooling and after PWHT are shown in Figs. 6A and 8, respectively.

An overall hardness value for the intercritical structure was HV 225. However, because the carbon content of the transformed regions was necessarily higher than in the overall material, considerable variation was noted in the as-simulated microstructure. An average microhardness of HV 280 (100 g) was found for the transformed regions. After PWHT, it was not possible to distinguish the transformed regions optically; the av-

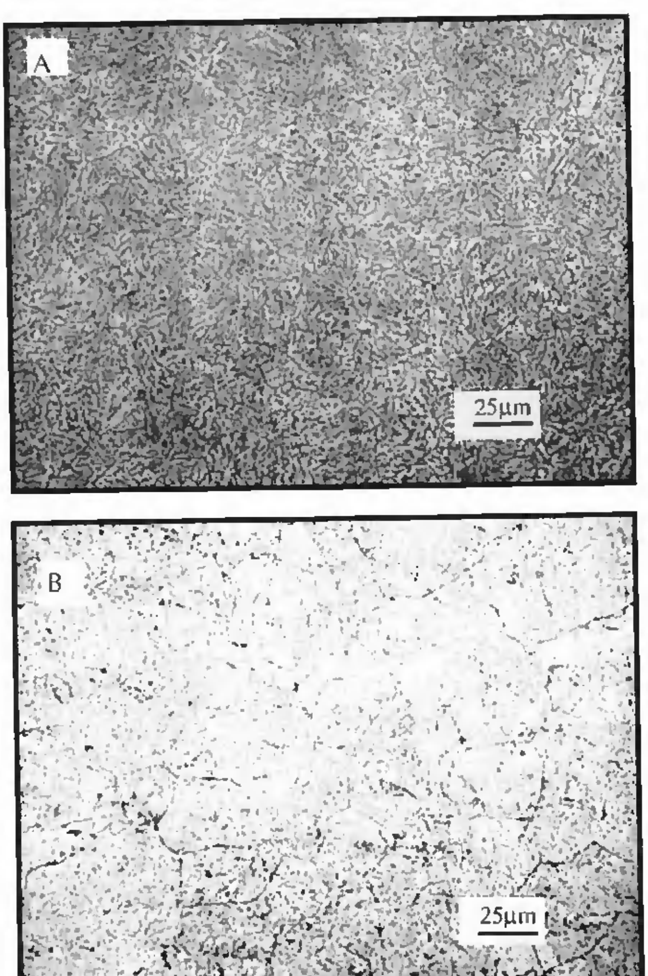

Fig. 4 — A — As-simulated coarse-grained microstructure; B — after PWHT. 4% Picral.

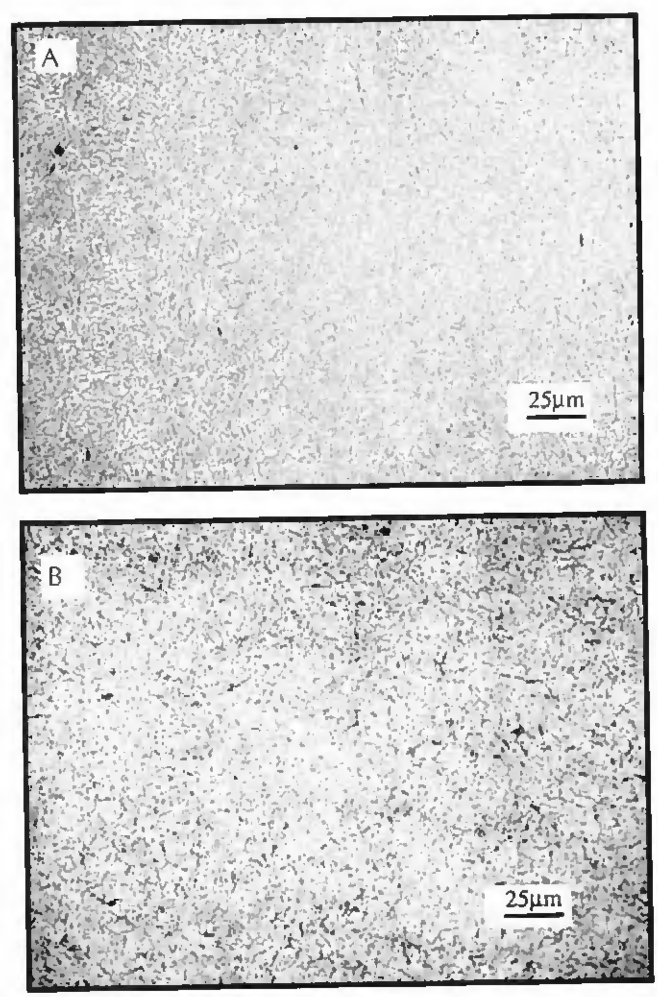

Fig. 5 — A — As-simulated grain-refined microstructure; B — after PWHT. 4% Picral.

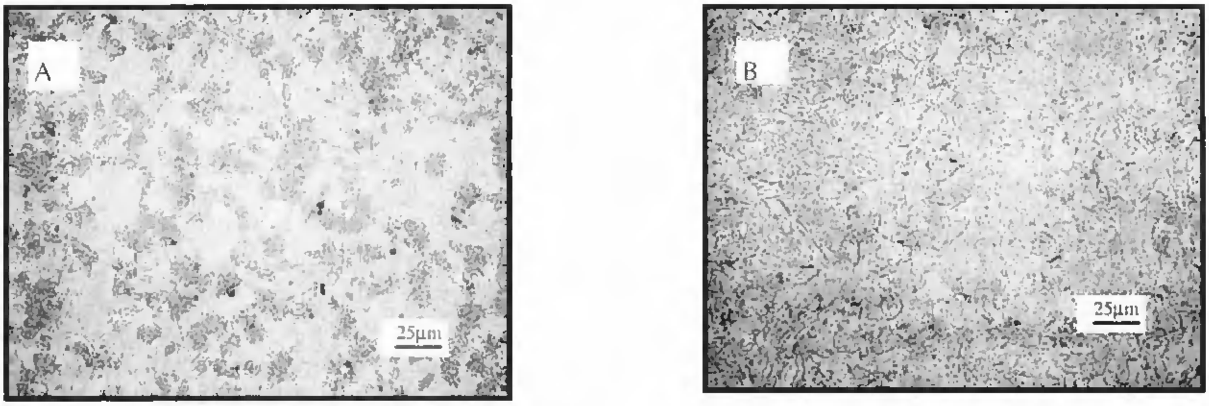

Fig. 6 — A — As-simulated intercritical microstructure; B — after PWHT. 4% Picral.

erage hardness of this microstructure was HV 185.

CDR Testing

In the mid-1970s, J. Pepe (Ref. 7) developed a short-time test that was based on the constant-displacement-rate testing of a notched-bar geometry. The test was capable of determining the long-time, notch-sensitivity tendencies of 1Cr-1Mo-0.25V rotor-forging materials.

Pepe noted that the elevated-temperature rupture strength is a typical design parameter and can be estimated by using the Larson-Miller parameter. However, no accelerated test had been developed to predict long-time notch sensitivity, even though adequate notch sensitivity is "crucial to insure reliable component operation within design life."

Figure 7 depicts the generalized load-displacement information obtained from CDR testing. A notched bar was elongated at a constant rate at a temperature near the upper service temperature of the material. Force, monitored during deformation, was seen to rise to a peak value; beyond the peak value, crack propagation led to a reduction in cross-sectional area and a decrease in force. The displacement rate was low, 0.05 mm/h (0.002 in./h), and was measured at the notch; this allowed for stable crack growth up to failure. Displacement-at-failure was defined as the displacement at a lower force limit, which was chosen as 445 N (100 lb).

Parallel to the CDR tests, constant-load rupture tests were conducted by Pepe on both smooth and notched bars of CrMoV material. Stress values were calculated for the full diameter of the smooth bar and for the reduced cross-sectional area of the notched bar; thus, the notched bar was seen to exhibit greater strength initially. For brittle materials, premature crack formation led to early failure in the notched bar. A cross-over time was noted beyond which the notched bar exhibited lower rupture strength than the smooth bar. An empirical correlation was developed between the displacement-at-failure values of the CDR test and this

Table 2 — Results of Gleeble CDR Testing

Microstructure	Time at Failure (10^4 s)	Displacement at Failure mm (0.001 in.)	Peak Force ±1/4% kN (lb)	Slope after Peak Force, kN/mm (lb/0.001 in.)
Base metal	1.02	0.72 (28)	9.52 (2140)[a][b]	−13 (−76)
	1.10	0.78 (31)	9.25 (2080)	−12 (−70)
average	1.06	0.75 (30)	9.39 (2110)	−13 (−73)
Coarse-grained	0.57	0.40 (16)	10.1 (2260)[a]	N/A
	0.64	0.45 (18)	10.5 (2360)	N/A
average	0.61	0.43 (17)	10.3 (2310)	N/A
Grain-refined	1.11	0.78 (31)	9.21 (2070)[a]	−16 (−93)
	1.10	0.78 (31)	8.45 (1900)[b]	−17 (−96)
average	1.11	0.78 (31)	8.85 (1990)	−17 (−95)
Intercritical	1.24	0.87 (34)	8.63 (1940)[a]	−10 (−59)
	1.18	0.83 (33)	8.81 (1980)[b]	−12 (−67)
average	*1.21*	*0.85 (34)*	8.72 (1960)	−11 (−63)

(a) Shown in Fig. 8.
(b) Used for Fig. 14.

Table 3 — Results of Instron CDR Testing

Microstructure	Time at Failure (10^4 s)	Displacement at Failure mm (0.001-in)	Peak Force ±45N (10 lb) kN (lb)	Slope after Peak Force, kN/mm (lb/0.001 in)
Base metal	6.3	0.89 (35)	1.7 (380)	−0.9 (−5)
Coarse-grained	1.1	0.15 (6)	1.6 (360)	N/A
Grain-refined	7.7	1.09 (43)	1.2 (274)	−0.7 (−4)
Intercritical	6.7	0.94 (37)	1.3 (290)	−0.7 (−4)

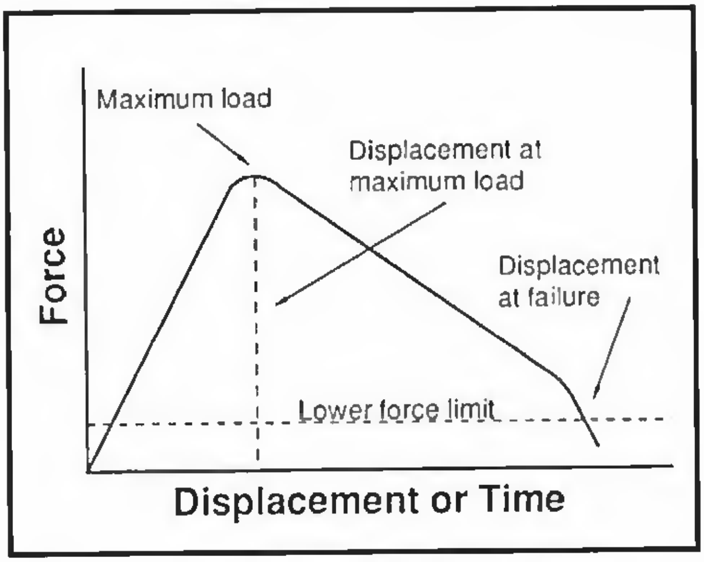

Fig. 7 — Generalized load-displacement curve from CDR test.

crossover-time parameter in the conventional, stress-rupture tests.

Implementation of the CDR test on the Gleeble was accomplished by W. F. Savage (Ref. 8); the test had been developed on an Instron testing machine. His tests of 1.25Cr-0.5Mo weld and base metals were conducted at a displacement rate of 0.25 mm/h (0.01 in./h). He noted that CDR testing could be conducted in the range of 0.05–0.25 mm/h (0.002–0.01 in./h) without strain-rate effects.

Experimental Procedure

Gleeble CDR testing

CDR testing on the Gleeble was controlled by a computer; a data-acquisition system recorded temperature, force on the test specimen, and crosshead speed. The programmed crosshead speed was 0.25 mm/h (0.01 in./h). A 650°C (1202°F) test temperature was maintained at the root of the notch in the specimen.

It was felt that a thermocouple welded at the root of the notch would affect the test results; therefore, direct temperature measurement was not possible. Preliminary tests were performed with thermocouples at the root of the notch and on the outer diameter of the bar, within 1 mm of the edge of the notch. It was determined that a temperature of 650°C at the root of the notch corresponded to 635°C (1175°F) at the outer thermocouple. This temperature, 635°C, was used for temperature control with the Gleeble.

In the actual test, temperature at the controlling thermocouple was linearly increased to 635°C in 2 min. This temperature was held for 2 min prior to the commencement of the crosshead displacement. For all tests completed on the Gleeble, fracture occurred after peak load, but before the load had decreased to the 445-N (100-lb) limit. When the test specimen fractured, the electrical circuit of the Gleeble was broken, data acquisition ceased, and the machine turned itself off. The crosshead was manually retracted, and the specimen was removed after it had cooled to room temperature.

Instron CDR testing

For testing in the Instron Model 8562, the specimen was positioned in threaded, stainless steel grips. A cross-wire-welded thermocouple was cemented to the specimen such that its tip was positioned next to the notch. A furnace attachment, consisting of six molybdenum-disilicide heating coils behind alumina brick, surrounded the specimen during testing.

As the furnace heated to 650°C prior to testing, the crosshead of the Instron was retracted so as to maintain a force of 89 N (20 lb) on the test specimen. The displacement rate, 0.05 mm/h (0.002 in./h) was measured at the notch by an extensometer. The value of the force was monitored past peak load and down to 178 N (40 lb). If the specimen had not fractured prior to this limit, it was pulled to failure after the furnace had cooled to room temperature.

Results

Gleeble CDR testing

Duplicate CDR tests were performed on the Gleeble for base-metal samples and samples with microstructures representing the coarse-grained, grain-refined, and intercritical regions of the weld HAZ. Figure 8 depicts the results of one test for each of these four microstructural regions. Noted for each test were the peak force, and the time-at-failure value. Time-at-failure values were converted to displacement-at-failure values through the constant displacement rate.

Table 2 lists the results of the Gleeble testing. Included in this table is a calculation of the slope of the force vs. displacement curve after peak load. From Fig. 8, data in this region appeared linear.

Table 4 — Relative Service-Life Estimates Calculated from Displacement-at-Failure Values

Microstructure	Displacement at Failure (mm)	Normalized to Base Metal	Fourth Power of Normalized Value[a]
	Gleeble Tests		
Base Metal	0.75	0.75/0.75 = 1.00	$1.00^4 = 1.00$
Coarse-Grained	0.43	0.43/0.75 = 0.57	$0.57^4 = 0.11$
Grain-Refined	0.78	0.78/0.75 = 1.04	$1.04^4=1.17$
Intercritical	0.85	0.85/0.75 = 1.13	$1.13^4=1.65$
	Instron Tests		
Base Metal	0.89	0.89/0.89 = 1.00	$1.00^4 = 1.00$
Coarse-Grained	0.15	0.15/0.89 = 0.17	$0.17^4 < 0.01$
Grain-Refined	1.09	1.09/0.89 = 1.22	$1.22^4 = 2.25$
Intercritical	0.94	0.94/0.89 = 1.06	$1.06^4 = 1.24$

(a) This value is an estimate of the ratio of the crossover time exhibited in service by a particular microstructure compared to the crossover time of the base metal.

No slope was calculated for the coarse-grained region, which fractured near peak load.

The base-metal fracture surface is shown in Fig. 9A. Banding at the centerline of the baseplate is evidenced; the reduced cross-sectional area of the test bar was machined from the plate center. Figure 9B shows a longitudinal view of the test bar at the fracture surface. Damage is noted within a banded region. Distorted grains reveal a ductile fracture.

Figure 10A shows the fracture surface of the coarse-grained test specimen. The lack of banding, like that present in the base-metal sample, is due to the weld thermal cycle and tempering required to achieve the coarse-grained structure. Evidence of crack propagation appears as a thin annular ring at the outer circumference of the fracture surface. Fast fracture occurred toward the center of the fracture surface. Both coarse-grained test specimens exhibited little ductility and fractured shortly after attaining peak load.

The intergranular nature of the fracture of the coarse-grained region is seen in Fig. 10B, which shows a longitudinal view of the test bar near the fracture surface. Cracks are noted along the boundaries of individual grains both at and below the fracture surface. Impurity segregation to these boundaries and the solution of alloying elements within the grains during thermal cycling can aid in promoting intergranular fracture.

Figure 11A shows the fracture surface of the grain-refined region. As with the coarse-grained region, no evidence of banding was detected. The refined structure is seen in a longitudinal view near the fracture surface — Fig. 11B. Cavities associated with deformation are noted below the fracture surface.

The intercritical-region fracture surface is seen in Fig. 12A. This microstructure exhibited greater ductility than that of the base metal; this is most likely due to the large amount of untransformed and retempered bainite present. Figure 12B shows a longitudinal view near the fracture surface. Significant deformation damage is seen below the fracture surface.

An examination of the average values of peak force from Table 2 ranked the coarse-grained region highest at 10.30 kN (2310 lb). In general, the maximum load is directly proportional to the ability of a material to resist creep deformation at elevated temperature. The coarse-grained value is nearly ten percent above the base-metal value of 9.39 kN (2110 lb).

The higher value measured for the coarse-grained material is noteworthy in that there is a difference of only one ASTM grain size number between the two microstructures. Other effects resulting from the coarse-grained thermal cycle may have played a role in the load difference. Greater amounts of alloying elements may have been put into solution. Also, thermal cycling eliminated the banding that was prevalent at the base-metal fracture surface. These effects could have acted to increase the strength of the coarse-grained microstructure.

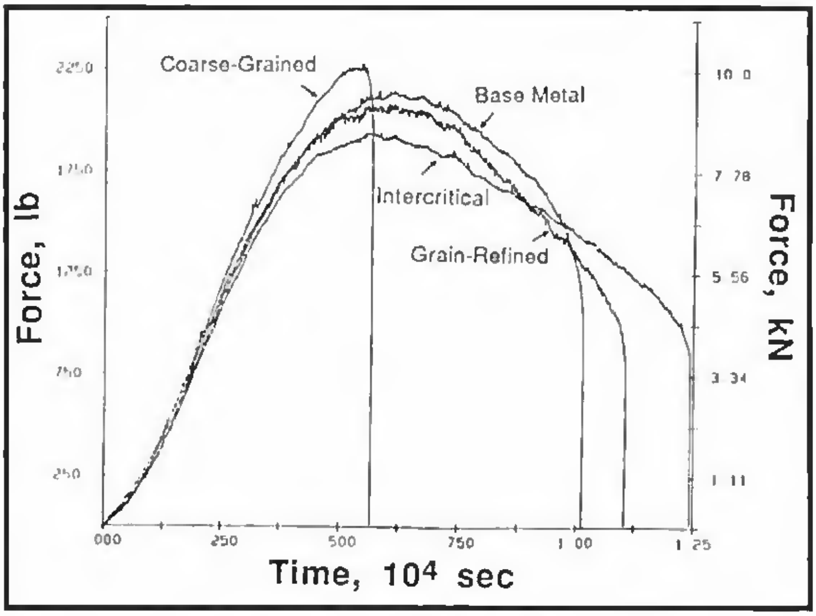

Fig. 8 — Load displacement curves from Gleeble CDR tests.

The grain-refined and intercritical regions exhibited the lowest average values of peak load, 8.85 kN (1990 lb) and 8.72 kN (1960 lb), respectively. The peak-load values from the tests of the two grain-refined tests bracketed the intercritical values. An overall observation is that the coarse-grained region exhibited the highest peak load, while the grain-refined region exhibited one of the lowest. This result was in accordance with the theory that increasing grain size imparts higher strength and improved creep resistance at elevated temperature (Ref. 9).

Also noted for the Gleeble tests was that the peak load for all microstructures occurred near a displacement of 0.43 mm (0.017 in.). Pepe (Ref. 7) noted a similar trend for CrMoV materials tested in the Instron. He observed that the peak loads occurred at approximately 0.15 mm (0.006 in.). Steel composition and specimen geometry may play a role in the variation of these displacement-at-peak-load values.

The reverse of the peak force results was observed for displacement-at-failure values (Table 2), which in this test were an indication of the notch-sensitivity tendencies of the microstructures. The inter-

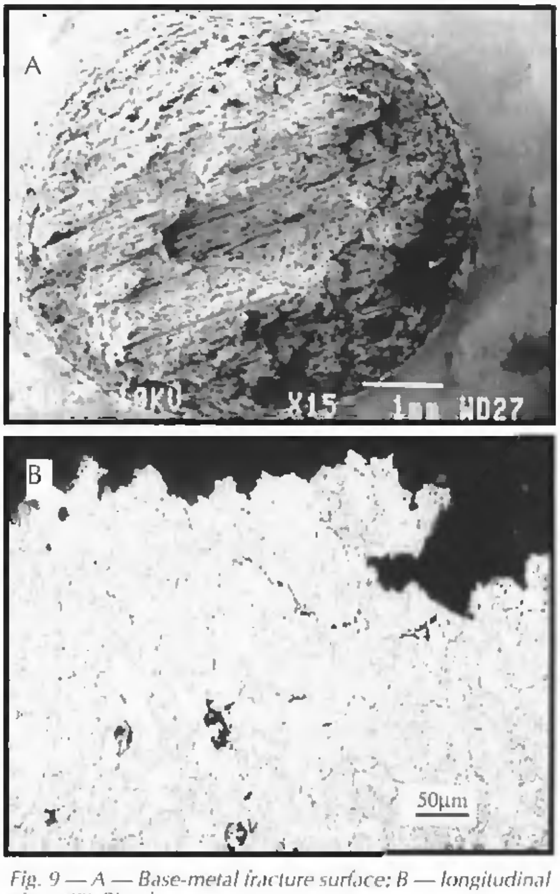

Fig. 9 — A — Base-metal fracture surface; B — longitudinal view, 4% Picral.

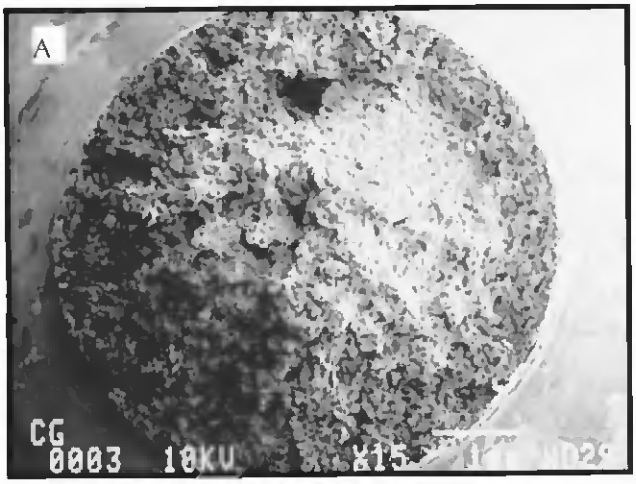

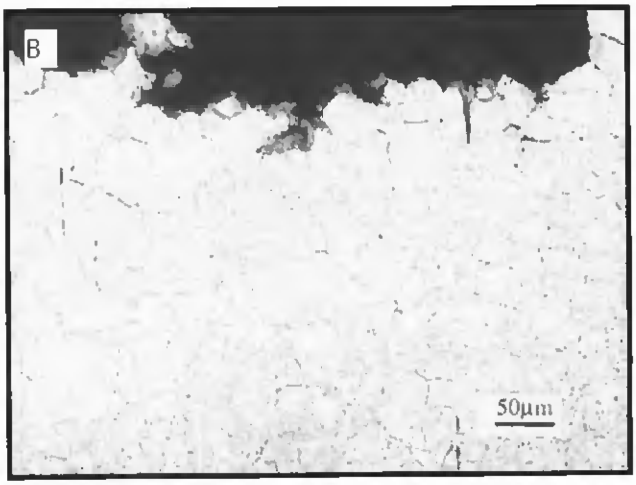

Fig. 10 — A — Coarse-grained-microstructure fracture surface; B — longitudinal view. 4% Picral.

critical region exhibited the greatest average displacement-at-failure, 0.85 mm (0.034 in.). The coarse-grained region exhibited the smallest displacement value, 0.43 mm (0.017 in.). These observations agree with the general observation that as the strength of a metal increases, its ductility decreases.

The slope-after-peak-load values (Table 2) clearly separated the microstructural responses. The grain-refined region exhibited the largest negative value of slope. This fast load loss with increasing deformation was felt to arise from the presence of small grains, which do not impart any great resistance to creep at elevated temperatures. The slope-after-peak-load values are quite close for the grain-refined tests even though the peak load values show nearly a 10% scatter. It should be noted that high-temperature properties can show considerable scatter, and measurably different results frequently are obtained between different heats of the same material or even between bars of the same heat (Ref. 10).

Instron CDR testing

Instron CDR tests were performed for comparison with the data obtained from the Gleeble tests. One test bar from the base metal and each of the HAZ microstructural regions was tested. Force and displacement data were monitored on a strip chart and an X-Y recorder. As with the Gleeble tests, peak load and time-at-failure were measured — Table 3. Figure 13 depicts the force vs. displacement data read from the X-Y recorder. The Instron extensometer control at the notch was able to maintain stable crack growth well past the peak force. Force was measured down to 180 N (40 lb) after peak load.

As with the Gleeble tests, the coarse-grained microstructure showed a precipitous drop in force shortly after peak load and exhibited the smallest displacement-at-failure value. In this Instron test, however, it was observed that this region exhibited a slightly lower peak load than the base metal. Additional testing would provide further data for verifying the true relative values of the peak loads.

The base metal exhibited a peak load of 1.7 kN (380 lb). The grain-refined and intercritical microstructures had values approximately 75% of this value. These

Table 5 — Sample Results of K_I Analysis of CDR Data

Load (kN)	Displacement (mm)	d[a] (mm)	K_I (MPa$\sqrt{m}$)	r[b] (mm)	strain rate (s^{-1})
		Gleeble Tests			
Base Metal					
9.2	0.51	6.2	14.5	0.90	3.9×10^{-5}
8.5	0.57	6.0	14.1	0.87	4.1×10^{-5}
Grain-Refined					
8.4	0.48	6.3	12.8	0.72	4.9×10^{-5}
7.5	0.61	6.0	12.5	0.69	5.1×10^{-5}
Intercritical					
8.7	0.45	6.3	13.4	0.79	4.4×10^{-5}
7.4	0.59	5.8	12.9	0.72	4.9×10^{-5}
		Instron Tests			
Base Metal					
1.6	0.36	2.8	7.5	0.25	2.8×10^{-5}
1.2	0.71	2.4	7.4	0.24	2.9×10^{-5}
Grain-Refined					
1.2	0.25	2.8	5.5	0.13	5.4×10^{-5}
0.68	0.91	2.1	5.2	0.12	5.9×10^{-5}
Intercritical					
1.2	0.30	2.8	5.7	0.14	5.0×10^{-5}
0.77	0.76	2.2	5.5	0.13	5.4×10^{-5}

(a) d is the remaining ligament diameter.
(b) r is the plastic zone radius at the crack tip.

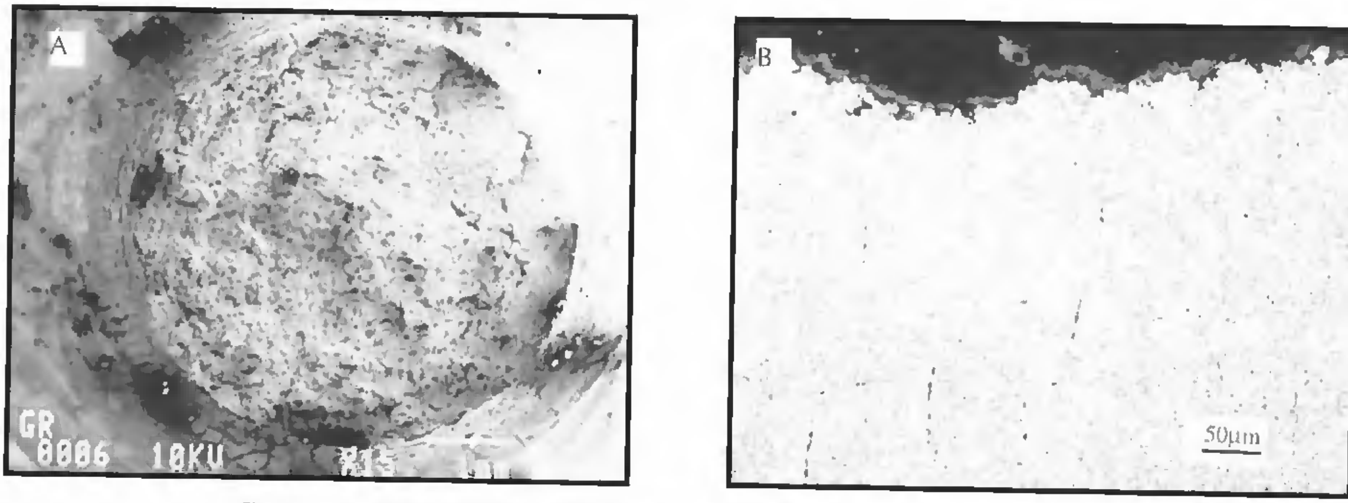

Fig. 11 — A — Grain-refined-microstructure fracture surface; B — longitudinal view. 4% Picral.

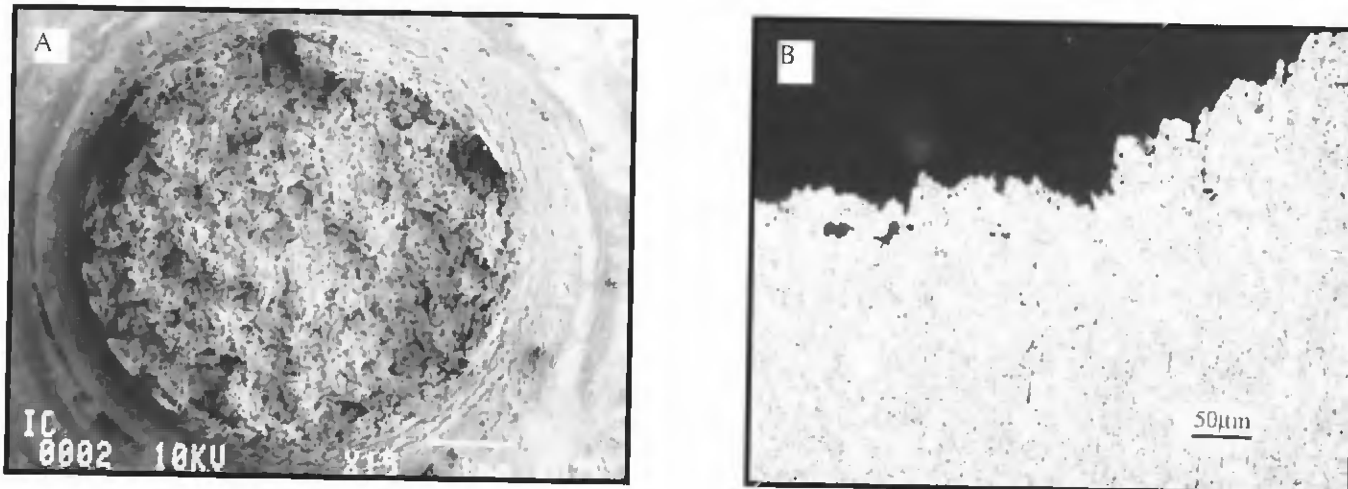

Fig. 12 — A — Intercritical-microstructure fracture surface; B — longitudinal view. 4% Picral.

microstructures with the lowest peak-force values exhibited the greatest displacement-at-failure.

Discussion

Service-Performance Estimation

As was mentioned previously, an empirical correlation was developed between the displacement-at-failure value in the CDR tests and the crossover-time parameter in stress-rupture tests of smooth and notched bars. Pepe (Ref. 7) used this relationship to predict the elevated-temperature service performance of candidate 1Cr-1Mo-0.25V steels for turbine rotors. This relationship was a function of the fourth power of the displacement-at-failure value.

Although no specific algorithm has been developed for 2.25Cr-1Mo steel, Savage (Ref. 8) extended the fourth-power relationship for use in 1.25Cr-1Mo steels. In the present case, this relationship will allow a qualitative assessment of the Gleeble and Instron data.

Table 4 lists the average value of the displacement-at-failure for the microstructures examined in the Gleeble and CDR tests. The values are then normalized to the values for the base metal. The final column shows the fourth power of this normalized value. These values represent the percentage of the crossover time relative to the base metal that the given microstructure would be expected to exhibit in service.

From this analysis, it was seen that the coarse-grained-HAZ microstructure is the service-life-limiting region. For Gleeble tests, it showed only 11% of the crossover time of the base metal; for the Instron tests, that number fell to less than 1%.

Gleeble testing revealed the intercritical region to have 165% of the crossover time of the base metal. For the Instron testing, the grain-refined region exhibited the largest value of displacement at failure. By the fourth-power relationship, it was seen to have 225% of the crossover time of the base metal.

Comparison of Gleeble and Instron CDR Test Results

There was correspondence between the results of the Gleeble and Instron CDR tests. Both methods identified the coarse-grained microstructure, with its low displacement-at-failure value, as the service-life-limiting region of the HAZ. The base metal was seen in both tests to have a good combination of peak force and displacement at failure. The grain-refined and intercritical microstructures exhibited the longest expected service life; however, they also had the lowest peak force values. As such they were identified as strength-limiting regions.

The two test methods exhibited a difference in the appearance of the load-displacement curves. A source of this difference is the type of displacement control. Control at the notch allowed for stable crack growth past peak load and down to near zero force in the Instron test. Crosshead control in the Gleeble tests also resulted in the tests continuing past

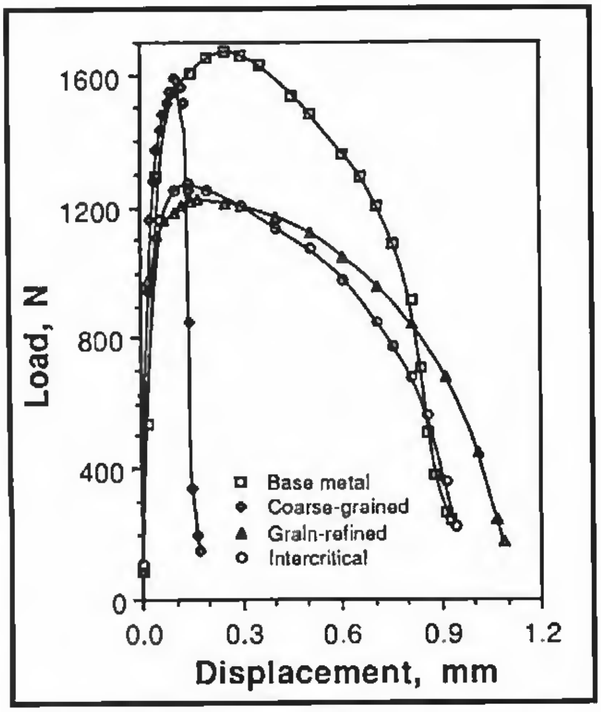

Fig. 13 — Force-displacement data from Instron CDR tests.

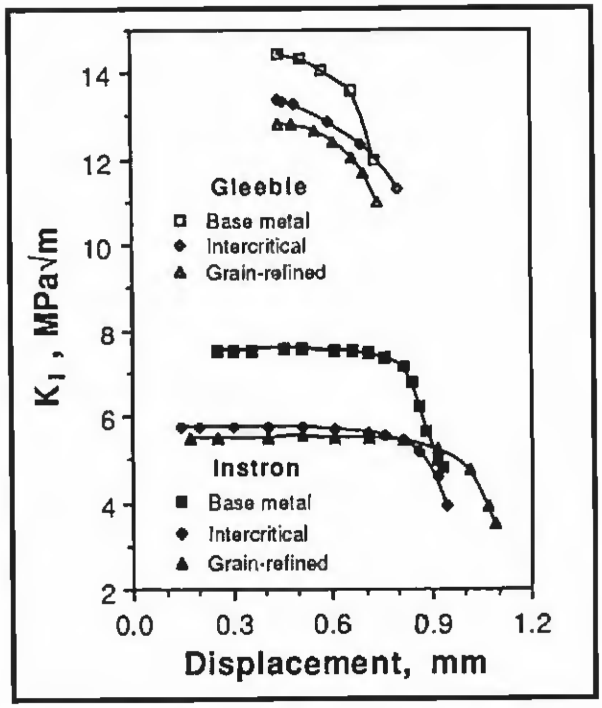

Fig. 14 — Results of K_I calculations from Gleeble and Instron CDR tests.

peak load, however, fracture occurred before the test specimen achieved lower force levels. The effects of resistive vs. furnace heating can also be considered.

As such, discernment between displacement-at-failure values for the most ductile microstructures, the grain-refined and intercritical regions in the present case, was best accomplished with the Instron. Nonetheless, the results of the Gleeble tests were readily interpreted to distinguish between ductile and brittle microstructures. Moreover, it is possible to outfit the Gleeble with an extensometer similar to the one used with the Instron and thus eliminate the control difference between the tests.

Variation of the peak temperature within the intercritical region would result in differing amounts of transformation product. The limiting amounts of transformation in this region are the base metal, which has no transformation product, and the grain-refined region, which is fully transformed. Therefore, test specimens with microstructures simulated for different intercritical peak temperatures could produce a wide array of results, especially if one of the microstructural constituents was martensite.

K_I Analysis

Stress intensity factors were calculated for the cylindrical, notched-bar geometry according to the equation (Ref. 11)

$$K_I = [P/D^{3/2}][1.72(D/d)-1.27]$$

where P is the load, D is the outer bar diameter and d is the remaining ligament diameter. Past peak load, it was assumed crack growth was occurring. From the results of Pepe (Ref. 7), the stress value at peak load was considered constant throughout the remainder of the test. Calculations of the remaining ligament diameter were based on the stress at peak load.

Figure 14 depicts the results of the K_I calculations. The values begin at peak load and are plotted against displacement. K_I values for the base metal were noted to be higher than for the grain-refined or intercritical microstructures. The Instron values show a slow initial degradation compared to the Gleeble values; this may be an artifact of the displacement control, which was more precise on the Instron machine. The sudden drop in the curve for the Instron tests parallels the drop in the force values — Fig. 13.

From the K_I values, it was possible to calculate a plastic-zone size at the crack tip, assuming plane strain, according to the formula (Ref. 12)

$$r \approx K_I^2/6\pi\sigma_{ys}^2$$

where r is the radius of the plastic zone and σ_{ys} is the flow stress at the testing temperature. An effective strain rate was found by dividing the displacement rate by the diameter of the plastic zone.

A flow stress value of 110 MPa (16 ksi) was used in the plastic-zone calculation. This value (Ref. 13) is for 2.25Cr-1Mo in the annealed condition at a testing temperature of 650°C. The value for the annealed steel was considered a lower limit for the yield strength and resulted in an overestimate of the plastic-zone size. This overestimate allowed for a conservative test of the plain-strain assumption.

Table 5 gives the results of sample calculations for different microstructural regions for both Gleeble and Instron tests. In all cases the plastic-zone size was revealed to be small compared to the remaining ligament diameter. As such, small scale yielding criteria were adhered to throughout the test. This observation supports the use of the K_I analysis for the CDR test results.

Despite the difference in displacement rate between the two test methods, the stain rate calculations for Table 5 yield similar values. This rate was calculated by dividing the displacement rate by the diameter of the plastic zone, 2r. These results support the initial idea that CDR testing can be conducted with displacement rates from 0.05-0.25 mn/h without strain-rate effects.

In fatigue testing it is common to relate the crack growth rate per cycle to the difference in the K value seen in each cycle according to the equation (Ref. 4)

$$da/dn = c(\Delta K)^m$$

where da/dn is the crack growth rate per cycle, and c and m are material constants. Erdogan (Ref. 15) modified this equation by multiplying it by the term $K_{max}{}^n$, where n is a constant, because it was noted that the crack growth rate increased with increasing values of the maximum K value for each cycle.

The data from this investigation were treated in a similar manner. The crack-growth rate, (dc/dt), was considered to be proportional to some power of K. An average crack growth rate was obtained by subtracting the final ligament radius from the initial radius and dividing by the test time. Proportionality constants were eliminated by taking ratios of the average crack-growth rates and K values. For CDR testing of the base-metal microstructures, the crack-growth rate was found to be proportional to K^3.

This sort of analysis may provide an insight into the empirically derived algorithm involving the fourth power of the displacenient-at-failure value. In service, the effective K values experienced at cracks would differ from those in CDR testing. The fourth-power relationship may relate the magnitude of the difference in K values as it relates to crack growth.

Life Assessment

The traditional approach to life assessment is to plot stress-rupture data vs. the Larson-Miller parameter. With an increasing number of power plants and refineries approaching their initial design-life estimates, however, research in the area of residual life prediction or life extension is offering new methods of evaluation.

Manjoine (Ref. 16) provides a method for the evaluation of creep-fatigue damage. The method derives constituitive relationships from tensile, creep-rupture and fatigue data obtained over a range of temperatures and from creep-fatigue tests. Further analysis, which considers design loads and transients such as plant startup and shutdown, are used to determine design or residual life. Viswanathan (Ref. 17) provides a compendium of life-assessment techniques for high-temperature components. Detailed therein are the problems associated with crack-initiation- and crack-growth-based life assessment.

As has been discussed, CDR testing was used to assess the long-time, notch-sensitivity tendencies of 1Cr-1Mo-0.25V rotor-forging materials. The empirical relationships derived for the evaluation of those materials were extended to evaluate 1.25Cr-0.5Mo weld and base metals. The present work continues the appliction of CDR testing to evaluate 2.25Cr-1Mo steel HAZ microstructures. Further development work is required to derive the relationships necessary to evaluate long-term notch sensitivity of specific materials.

Conclusions

Constant-displacement-rate (CDR) testing was employed to investigate the mechanical response of the base-metal and weld HAZ microstructures in 2.25Cr-1Mo steel to elevated temperature deformation. It was concluded that the CDR test is an effective, short-time procedure to delineate and compare the strength and relative service life of the structures present in the HAZ of 2.25Cr-1Mo steel.

This investigation comprised an initial foray into the comparison of CDR testing on a Gleeble and an Instron. The results of this research, which represented testing simulated HAZ microstructures in single-pass welds, should act as a baseline for research into the effect of multipass welds and weld repair on HAZ mechanical properties. Also, factors were identified, such as specimen geometry and displacement control, which warrant further study.

The coarse-grained microstructure exhibited the lowest value of displacement-at-failure and was thus identified as having the greatest notch sensitivity and shortest expected service life. Based upon a fourth-power relationship between displacement-at-failure and crossover time, Gleeble tests revealed this region to have a service-life estimate of approximately 11% of the unaffected base metal.

The grain-refined and intercritical regions exhibited the largest values of displacement at failure in the CDR testing. However, peak-load observations revealed these HAZ regions to be strength-limiting.

Calculations of the plastic-zone size revealed it to be smaller than the remaining ligament. Therefore, small-scale-yielding criteria were adhered to throughout the CDR testing of 2.25Cr1Mo steel in this investigation. This fact supports the use of a K_I analysis.

K_I values obtained from Gleeble CDR testing were nearly double the values from Instron CDR testing. This fact is due to the different specific notched-bar geometries used in the two tests. Both the Gleeble and Instron tests showed the base metal to have the highest K_I value.

Although the crosshead control of the Gleeble is not as sensitive to notch displacement compared to the extensometer control of the Instron, the results of the Gleeble tests were easily interpreted to reveal ductility trends in the HAZ microstructures.

Acknowledgments

The authors wish to thank Dynamic Systems, Inc., formerly Duffers Scientific, Inc., Poestenkill, N.Y., and D. VanSteele for their aid in the experimental testing and many constructive discussions.

References

1. Smith, G. V. 1971. Supplemental report on the elevated-temperature properties of chromium molybdenum steels (an evaluation of 2.25Cr-1Mo steels), ASTM Data Series, DS 6S2, American Society for Testing and Materials.

2. Lundin, C. D., and Wang, Y. 1989. Repair welding of service exposed Cr-Mo steel weldments, Welding Research Council Bulletin 348, November.

3. Lundin, C. D., Kruse, B. J., and Pendley, M. R. 1982. High temperature properties of 2.25Cr1Mo weld metal, Welding Research Council Bulletin 277, May.

4. Lundin, C. D., Khan, K. K., Yang, D., Hilton, S., and Zielke, W. 1990. Failure analysis of a service-exposed steam line in a utility steam plant, Welding Research Council Bulletin 354, June.

5. Nippes, E. F., Merrill, L. L., and Savage, W. F. 1949. Cooling rates in arc welds in 1/2-in. plate, *Welding Journal*, 28(11): 556-s to 564-s.

6. ANSI/AWS D10.8-86, *Recommended Practices for Welding Chromium Molybdenum Steel Piping and Tubing*, American Welding Society, Miami, Fla.

7. Pepe, J. J., and Gonyea, D. C. 1989. Constant displacement rate testing at elevated temperature in fossil power plant rehabilitation. Proceedings of an International Conference, February 27 to March 1, 1989, Cincinnati, Ohio, sponsored by ASM International and ASME.

8. Savage, W. F., and Nippes, E. F. Unpublished notes, Materials Engineering Department, Rensselaer Polytechnic Institute, Troy, N.Y.

9. Dieter, G. E. 1976. *Mechanical Metallurgy*, p. 479. McGraw Hill Book Co., New York.

10. *Ibid.*, Dieter, p. 480.

11. *Ibid.*, Dieter, p. 511.

12. Hertzberg, R. W. 1983. *Deformation and Fracture Mechanics of Engineering Materials*, p. 292. John Wiley & Sons, New York.

13. *Metals Handbook*, 9th Edition: Volume 1. 1990. P. 655. ASM International, Materials Park, Ohio.

14. Meyers, M. A., and Chawla, K. K. 1984. *Mechanical Metallurgy: Principles and Applications*, pp. 710–715. Prentice-Hall, Inc., Englewood Cliffs, N.J.

15. Erdogan, F. 1967. Crack propagation theories, NASA-CR-910.

16. Manjoine, M. J. 1994. Simplified methods for creep-fatigue damage evaluations and the application to life extension, Welding Research Council Bulletin 394, August.

17. Viswanathan, R. 1989. *Damage Mechanisms and Life Assessment of High-Temperature Components*, ASM International, Metals Park.